ЯФ, 1966, т. 4, в. 2, 24/II-66
с. 342-356.

ОБЪЕДИНЕННЫЙ
ИНСТИТУТ
ЯДЕРНЫХ
ИССЛЕДОВАНИЙ

Дубна

E - 2517

V.S.Evseyev, Chang Run-hwa, V.A.Chernogorova,
V.S.Roganov, M.Szimchak

ANGULAR DISTRIBUTION OF HIGH ENERGY NEUTRONS EMITTED IN ABSORBING POLARIZED μ^--MESONS IN CALCIUM

1965

E - 2517

V.S.Evseyev, Chang Run-hwa, V.A.Chernogorova,
V.S.Roganov, M.Szimchak

ANGULAR DISTRIBUTION OF HIGH ENERGY NEUTRONS EMITTED IN ABSORBING POLARIZED μ^--MESONS IN CALCIUM

Submitted to JNP

INTRODUCTION

For the first time it has been shown by L.S.Shapiro, L.D.Blokhintsev, E.I.Dolinsky [1] and later by other authors [2-9] that the study of the angular distribution of neutrons produced in mu^- meson absorption by Z nucleus

$$\mu^- + Z \to (Z-1) + n + \nu \qquad (1)$$

can give valuable information on parity nonconservation and coupling constants in the simple mu^- meson absorption by free protons

$$\mu^- + p \to n + \nu \,. \qquad (2)$$

Due to total mu^- meson depolarization in hydrogen [10] at density necessary for carrying out the experiment the angular distribution of neutrons in process (2) seems to be impossible to investigate at present.

Neutrons produced in process (1) can be emitted either via the compound nucleus ("evaporation" neutrons) or missing the stage of the compound nucleus ("direct process" neutrons).

The angular distribution of the direct process neutrons is of the form [1-9]

$$N(E,\theta) = 1 + B\cos\theta$$
$$B = \alpha(E)\beta(E)P_\mu \,, \qquad (3)$$

where $N(E,\theta)$ is the number of neutrons of the energy E emitted at an angle θ, θ is the angle between the neutron pulse and the mu^- meson spin, B is the asymmetry coefficient, P_μ is the residual polarization of mu^- mesons at the K-orbit of the mesic atom, $\alpha(E)$ is the factor depending only on coupling constants and the neutron energy E, $\beta(E)$ is the factor depending only upon the properties of a specific nucleus and neutron energy.

In studying neutron angular distribution it is necessary to take into account that the nucleus produced in mu^- capture, in general [6,7,9], emits "evaporation"

neutrons and gamma-quanta with isotropic angular distribution. Therefore, for detecting neutrons it is necessary to use a detector which is nonsensitive to relativistic particles and to choose the energy region in the neutron spectrum with the minimum contribution of evaporation neutrons.

Nearly in all the investigations on asymmetry in neutron angular distribution[11-19] use was made of threshold scintillation neutron detectors nonsensitive to electrons and gamma-quanta. The neutron detection threshold E_n was taken in earlier experiments in the (1.5 - 7.0) MeV range. For $E_n \lesssim 5$ MeV the contribution of evaporation neutrons is still of importance. The preliminary analysis of experiments at low thresholds is described in ref.[17].

The description is given of the method and the results of investigating the angular distribution of neutrons from the absorption of partially polarized mu^- mesons in Ca at various thresholds E_n in the energy range from 6.7 to 20.7 MeV. Earlier short information on the results of this experiment[18] was published.

Description of the Experimental Instruments

The apparatus with which the neutron angular distribution was studied had been described mainly by the authors of ref.[16]. In the present paper only new blocks of the apparatus are described in detail.

Mu^- mesons were detected and the moment of their stopping in a metallic Ca target 12 g/cm^2 (see Fig. 1) was found with a telescope of two scintillation counters 1 and 2. Mu^- decay electrons were detected with a telescope of three scintillation counters 3, 4 and 5. A laminated threshold scintillation detector nonsensitive to relativistic particles[20] was used for detecting neutrons. The target was inserted into a coil for obtaining mu^- meson spin precession.

Since the target was sufficiently thick for 90% of all the mesons to stop in it, whereas mu^- telescope counter No. 2 nearest to the target was placed close to the coil and had linear dimensions in the vertical plane 5x5 cm (the target was 12x12 cm in the same plane), it was necessary to have an anticoincidence counter around the target.

Coincidence pulses of the meson telescope T_μ were fed to the scaler to count mu^- mesons N_μ and the coincidence circuits $(\mu e)_{e+b.}$, $(\mu e)_{b.}$, $(\mu e)_{e+b.}$ and $(\mu e)_{b.}$. After being shaped the pulses from the electronic telescope T_e were fed to the coincidence circuits $(\mu e)_{e+b.}$ and $(\mu e)_{b.}$. The delay L_1 was taken so that with the help of the circuit $(\mu e)_{e+b.}$ one might detect

electrons in the time interval $t_e = 2\ \mu$ sec after $\Delta t_e = 0.1\ \mu$ sec on the mu^- meson arrival, i.e. to detect mu^- decay electrons and the random coincidence background N^e_{e+b}, whereas with the help of the circuit $(\mu e)_b$ to detect electrons in the interval $t_e = 2\ \mu$ sec before the mu^- meson arrival, i.e., the random coincidence background N^e_b.

The delay L_2 and the coincidence circuits $(\mu n)_{e+b.}$ and $(\mu n)_{b.}$ served for the same purpose. Pulses from the neutron detector (6) after being shaped by the block (f.p.) were fed not only to the circuits $(\mu n)_{e+b.}$ and $(\mu n)_{b.}$, but also to the linear integral discriminator (D). The discriminator together with coincidence circuits I and II and the delay L_3 allowed to count the random coincidence background N^e_b and the neutrons from calcium together with the background $N^n_{e+b.}$ at a given energy threshold E_n. To know N^n_{e+b} and N^n_b is necessary only for checking up the instruments.

The time and amplitude distribution of pulses of the neutron detector was investigated by detecting meson and neutron pulses with a cathode ray tube (CRT). The pulse triggering CRT sweep came from the coincidence circuit output $(\mu n)_{e+b.}$. Simultaneously the same pulse, corresponding to the time T_μ meson telescope one, was fed to the vertical deflecting plates of CRT. A pulse from the neutron detector was also fed to the same plates. Delays were chosen so that a meson telescope pulse was at the beginning of the sweep, whereas the working part of the sweep corresponded to the investigated time interval $t_n = 1\ \mu$ sec after the meson pulse arrival. To avoid the overlapping and distortion of pulses at short distances the sweep neutron detector pulses were delayed $\Delta t = 0.1\ \mu$ sec with respect to the meson pulse. $\Delta t = 0.1\ \mu$ sec was taken in order not to register neutrons emitted from the mu^- in the copper winding of the precession coil.

Use was made of the English telescope WM2LF/1. Pictures were taken with a RF-3 film 35 mm wide of 1000 GOST sensitivity moving at a speed 10 cm/min with a "YUPITER" camera having a relative aperture 1:1.2. Fig. 2 shows a typical picture taken at the CRT screen. Pictures were scanned with a DI-A reprojector. The amplitude A of the neutron pulse and the distance L between meson and neutron pulses were measured in scanning. The error in measuring A and L with a reprojector by four scanners was ± 0.7 mm. The working interval of the value A was about 85 mm, the working interval for L was about 160 mm.

The events when there were two meson or two neutron pulses at the sweep were rejected. They were about 1% and were uniformly distributed at the sweep.

The effect of the A pulse amplitude upon the value L was studied specially. For this purpose pictures were taken in conditions when particles simultaneously hit the neutron detector and the meson telescope. As was shown by scanning, L does not depend upon A over all the working range of L and A.

It was shown by photographing random coincidences for the chosen A working interval that the detection efficiency of the neutron pulse does not depend upon L (with the account of the nonlinear sweep) within 1.2% accuracy.

The sweep linearity and the absolute time scale were checked up during all the experiment by photographing a (10 ± 10^{-3}) MHz sinusoid as well as by means of ealier calibrated delays. The nonlinearity at the end of the L working interval was about 10%.

To measure the mu^- meson lifetime in Ca by means of decay electrons use was made of the time analyzer consisting of a (T → A) transformer and an amplitude analyzer. A convertor circuit is shown in Fig. 3. A time interval section is built on a 6A3 II tube. The tube is open on a third net and is shut on the first net. A long straight positive pulse, whose leading edge coincides in time with the moment of mu^- meson detection, enters input I of the circuit. The pulse triggers the tube. A long straight negative pulse, whose leading edge coincides in time with the moment of electron detection, enters input 2 and cuts off the tube. The anode resistance initiates a positive straight pulse. Its length is proportional to the time interval between the mu^- meson pulse and the electron one. After being inverted on a 6Ж9П tube (L_2) this pulse discharges the capacitance C in a circuit of the fantastron type on a 6Ж9П tube (L_3). The capacitance discharge occurs for the time equal to a negative pulse length and a negative pulse arises of an amplitude proportional to the negative pulse length at the input L_3. To reduce the time necessary for the curcuit to return to its initial state in the feedback the cathode follower (L_4) was used. The circuit provided the transformator linearity to a 1% accuracy.

Neutron and Electron Identification

It was stated that the removal of the target from the beam or the 2.5 shift of the studied time interval from the moment of the mu^- meson stopping caused the equal (within some per cent) counting of the pulses N^n_{e+b} and N^n_b after the $(\mu n)_{e+b}$ and $(\mu n)_b$ coincidence circuits, respectively. In this case a uniform neutron pulse (with the account of sweep linearity) distribution over the oscilloscope sweep was observed.

To make sure that the target effect is due just to mu^- capture in Ca and to check the correctness of calibration in time the mu^- meson lifetime in the target was measured both by electron and neutron countings at various thresholds E_n. Fig. 4 shows the dependence of the electron counting in time. The dependence was obtained with a T → A convertor. The background of random coincidences of some per cent from the counting at zero time and the background of plastic scintillators surrounding the target were subtracted. The background was measured in alternating a Ca target by a Pb one of identical thickness and geometry and was about 2% at zero time from the counting from the Ca target. The lifetime $\tau^e_{Ca} = (0.335 \pm 0.009).10^{-6}$ sec obtained in this way coincides with that obtained by Sens[21] $\tau_{Ca} = (0.333 \pm 0.007).10^{-6}$ sec.

When the lifetime τ_{Ca} was measured by detecting neutrons with the oscilloscope at various thresholds E_n the lifetime turned out to be equal and to coincide within errors (the error in τ_{Ca} at the lowest threshold E_n was 1.5 time larger than in measuring on electrons) with τ_{Ca} measured in an electron experiment (see Fig. 5).

To prove that high energy decay electrons having asymmetrical angular distribution are not registered in a laminated detector we measured, the same as earlier, the detection efficiency of gamma-rays of various energies, relativistic particles in cosmic rays, decay electrons from a light target with a neutron detector. In particular, in changing a Ca target by a carbon target N^n_{e+b} and N^n_b at large E_p were equal to an accuracy of some per cent. It follows from the experiments that the contribution of decay electrons from Ca to the neutron counting does not exceed 0.5% even at the highest threshold. At lower thresholds the contribution of decay electrons is still smaller since the number of recoil protons increases much faster with decreasing energy than decay electron counting.

In view of a considerable thickness of a Ca target in the direction of the neutron detector (1/2 of the target is about 7 g/cm^2) decay electrons emit bremstrahlung gamma-rays which can be, in principle, detected by a neutron detector on protons from the C^{12} (γ p) reaction in B^{12}. Simple calculation show that at the lowest threshold E_n = 6.7 MeV protons from a (γ p) reaction constitute only about 1% in the total proton counting. Their contribution is decreased approximately exponentially down to 0.01% for the highest neutron detection threshold E_n = 20.7 MeV.

It is known[22] that in mu^- capture in complex nuclei charged particles are emitted with a some per cent probability. In our case owing to a large target

thickness and the presence of a light filter in front of a neutron detector no appreciable number of these charged particles was detected.

The energy calibration of the neutron detector was made by gamma-rays of various energies, relativistic particles and neutrons of various energies up to 14 MeV obtained with an electrostatical accelerator. To pass from scintillation amplitudes caused by electrons to the amplitudes of proton oscillations use was made both of experimental data for a plastic scintillator E 102[23] and of our data[20], coinciding with them, for a home plastic scintillator having approximately the same constitution (polystyrene + 0.9% of p-terphenil + 0.05% of α NPO) as that of a E 102 scintillator.

Method of Measurements and Experimental Data Treatment

The anqular distribution of neutrons was studied by the precession method of mu^- meson spin in the magnetic field. Measurements without precession were performed for the sake of checking. On average the counting of mu^- meson stops was $N \approx 10^3$ 1/sec, the rate of taking pictures was about 20 sweeps per minute.

As a result of scanning the pictures time distributions for neutron pulses with an A amplitude were obtained. For each A amplitude the time distribution is

$$N_i(t_i) = N_o e^{-t_i/\tau_{Ca}} [1 + B \cos(\omega t_i + \delta)] + C \quad , \qquad (4)$$

where $N_i(t_i)$ is the number of events in the i-th time interval, t_i is the centre of the i-th time interval, ω is the precession frequency of the mu^- meson, δ is the angle between the mu^- meson spin direction at the moment of its stopping and the line connecting the centre of the target with that of the neutron detector, B is the asymmetry coefficient, N_o is the number of neutrons from Ca for $t = 0$, C is the random coincidence background, i is changed from 0 to 11.

The scanning data were treated in two ways. First, all the events with an A amplitude were treated which were larger than our selected values of A_k. Recoil proton energy corresponding to these values of A_k determined the thresholds E_n for neutron detection. Second, the overall working range A was divided into A_k intervals and the data on each interval were treated separately. In the first case data for various E_n are not independent, in the second case they are independent. A set of N_o numbers obtained in the second way of treatment for 15 intervals ΔE_n is just a differential recoil proton spectrum (see Appendix).

The mean neutron energy E for each threshold E_n or for each ΔA_k interval was calculated (see Appendix), knowing the dependence of the laminated neutron detector efficiency upon neutron energy and the threshold E_n, and also the spectrum of the direct neutron process.

By the least squares method with an electronic computer for various E_n and various ΔA (i.e. for various ΔE_n) the values N_o, B, C were determined with the given $\tau_{Ca} = (0.335 \pm 0.009) \cdot 10^{-6}$ sec, $\omega = 2\pi/0.74\ \mu$ sec (the precession magnetic field strength being about 100 Gauss) and $\delta = \pi/2$ (the errors N_i, t_i, τ_{Ca}, ω and δ were introduced into the electronic computer). The errors of the latter two values (about 2%) make a small contribution to the errors of N_o, B, C. The error of τ_{Ca} is most important.

Calculation results are given in Table 1. In the first six lines of the Table there are more accurate, compared to ref.[18], values of B for various E_n. From the seventh to the ninth lines there are independent values of B for various ΔE_n intervals.

When treated in the first way the value N_o/C changes from 3.5 for $E_n = E_n = 6.7$ MeV to 8 at $E_n = 20.7$ MeV, N_o at $E_n = 20.7$ MeV is 25 times smaller than for $E_n = 6.7$ MeV.

Fig. 6 shows an example precession curves for some values of E_n.

The asymmetry coefficient B measured without the precession field over the whole range of the values of A within (1.5 ± 3)% turned out to be equal to zero.

The residual polarization P_μ was determined by measuring the asymmetry coefficient in the angular distribution of mu^- decay electrons by the mu^- meson spin precession method in the magnetic field. The asymmetry coefficient was found 1) by calculating from the precession curve obtained with a $(T \to A)$ transformer and 2) by counting mu^- decay electrons in the time interval $t_e = 2\mu$ sec. After $\Delta t_e = 0.1\mu$ sec after the moment of the mu^- meson stop at two opposite in sign and equal values of the precession field, i.e. the same as in our ref.[16]. According to the second way

$$P_\mu = 3\,a(0)$$

$$a(0) = \frac{a(Ee)\,\nu}{Sb}, \qquad (5)$$

where a (0) is the asymmetry intergal coefficient for the case when all decay electrons are detected.

$a(E_e) = \frac{|N^e_{0.1\,e+b}|_+ - |N^e_{0.1\,e+b}|_-}{|N^e_{0.1\,e+b}|_+ + |N^e_{0.1\,e+b}|_-}$ is the asymmetry coefficient measured at the threshold E_e, $\nu = \frac{0.1 N^e_{e+b}}{N^e_b}$ at any direction of the precession field, S is a factor taking into account the increase of the measured $a(E_e)$ asymmetry with increasing E_e, b is the factor taking into account the asymmetry decrease due to electron detection during a large interval t_e /16/

$$ {}_e N^e = {}_{0.1} N^e_{e+b} - N^e_b - \frac{1.5 N^e_{e+b} - N^e_b}{d}, \qquad (6) $$

where ${}_{0.1}N^e_{e+b}$ is the electron counting with a $(\mu e)_{e+b}$ circuit at $\Delta t_e = 0.1\mu$ sec, ${}_{1.5}N^e_{e+b}$ is the electron counting with the same circuit at $\Delta t_e = 1.5\mu$ sec, where only the background N^e_b is counted (which is counted with a $(\mu n)_b$ scheme) and the "carbon" background due to counters in the vicinity of the target and the coil micarta carcas producing the precession field; d is the factor which makes it possible to take into account the background at $\Delta t_e = 0.1\mu$ sec.

Owing to a great thickness of the Ca target the spectrum of electrons emerging from the target and the integral asymmetry coefficient $a(E_e)$ were calculated by the Monte Carlo method[x]. Ionization and radiation losses of electrons in the target, multiple scattering and the contribution of various target parts with the account of the density of mu^- meson stops were taken into consideration in these calculations. The electron spectrum obtained in this way and $a(E_e)$ are shown in Fig. 7, $a(E_e)$ being corrected also by the Monte-Carlo method /24/ for radiation processes and multiple scattering in our three counter telescope.

The summed thickness of three plastic scintillators (3 cm) and two filters of the same material is 5.4 g/cm^2. This provides E_e = 10.4 MeV and according to the curve in Fig.7 S = 0.39/0.33 = 1.17.

The value a(0) was measured three times with a variation of the precession field sign at various "b" in the interval from 0.705 to 0.711 and various values of ν in the range from 2 to 2.44 and once with a (T → A) transformer. The counting rate was N^e_{e+b} = 10 1/sec. Thus, the following values of P_μ : 0.216 ± 0.028; 0.183 ± 0.022; 0.230 ± 0.032; 0.263 ± 0.043 have been obtained respectively.

---

x) The authors are thankful to W.Kusch for making these calculations.

The weighted mean of $P_\mu = 0.214 \pm 0.017$. A correction should be introduced which is due to asymmetry in the angular distribution of electrons emerging from a coil micarta carcas present in the precession field. This background is about 10 per cent from the counting of electrons from Ca in the interval $t_e = 2\,\mu$ sec at $\Delta t_e = 0.1\,\mu$ sec. The composition of the micarta is such that the counting of electrons from carcas is distributed equally between carbon and oxygen. P_μ for carbon and oxygen are close to P_μ for calcium. The coil consists of two carcases, the outer one being in the field two times smaller than that of the internal carcas. The correction for carcas background precession is only about 1.5% and the final value $P_\mu^{Ca} = 0.210 \pm 0.016$.

It should be noted that in measuring τ_{Ca} with a $(T \to A)$ transformer the "carbon" background was 5 times smaller due to the absence of the precession coil and the use of a specail circuit eliminating the detection of decay electron from μ^- mesons stopping in the nearest to the target counters of an electronic (T_e) and meson $(T\mu)$ telescopes.

Discussion of the Results

It follows from the data of Table I that for high energy neutrons B/P is close to its limit value - 1. This result was also reported in ref.[25]. To compare with theory Fig. 8 shows by dots with errors the dependence of the value $B/P\mu$ upon the mean enrgy $\bar{E}$, (Table 1); the solid curve shows the dependence $(\alpha\beta)$ upon neutron energy reported in ref.[27]. It should be noted that β is equal to unity in these calculations. The expression for the asymmetry coefficient can be written in the form[26]

$$\frac{B}{P_\mu} = \frac{G_V^2|M'_V|^2 - 2G_A^2|M'_A|^2 + (G_p - G_A)^2|M'_P|^2}{G_V^2|M_V|^2 + 2G_A^2|M_A|^2 + (G_P - G_A)^2|M_P|^2},$$

where $M'_{V,A,P}$ and $M_{V,A,P}$ are matrix elements depending upon the nuclear properties and G_V, G_A, G_P are effective coupling constants[26]. If $M'_V = M'_A = M'_P$ and $M_V = M_A = M_P$ (which is always suggested in the μ^- capture theory), then $B/P_\mu = \alpha\beta$, where one of the factors $\beta = \frac{|M'_V|^2}{|M_V|^2} \leq 1$ depends only upon the nuclear properties, whereas the other $\alpha = \frac{G_V^2 - 2G_A^2 + (G_P - G_A)^2}{G_V^2 + 2G_A^2 + (G_P - G_A)^2}$ depends only upon the interaction constants. If such a factorization is possible indeed, then for high energy neutrons it follows from our experiments that $\alpha \approx -1$ and $\beta \approx 1$. The coefficients β takes into consideration mainly two factors: proton motion in the nucleus and the interaction of the emerging neutron with a nucleus. Both the effects decrease asymmetry in the neutron angular distribution ($|\beta| \lesssim 1$)

The calculation of β by means of various nuclear models give entirely different values of β and various β dependences on neutron energy, but, perhaps, one may understand qualitatively the increase of the factor to unity with increasing neutron energy. Thus, e.g., in the calculations by means of the Fermi-gas [5] β reaches unity at a high energy end of the neutron spectrum.

If the result for β can be qualitatively explained on the basis of some model, then trying to account for a large value of α one faces great difficulties. The matter is that it follows from the μ^- capture theory [6,7] that for high energy neutrons $\alpha \approx -0.35$ if one takes into consideration some relativistic terms in the effective interaction Hamiltorian, and $\alpha \approx -0.1$ with the account of these terms made in ref. [27].

Making use of the conventional four interaction constant it is easy to show [18,28] that the value $\alpha \approx -1$ is possible only with considerable increasing of the ratios g_A/g_V and g_P/g_A.

An attempt was made [29] to explain the large value of α by introducing the weak interaction constant of the "second class" [30]. However, such an approach meets difficulties in numerical calculation of other effects in μ^- capture [31].

In view of the consequences important for theory to which the above interpretation of our result leads, special attention should be paid to the permissiblity of α and β factorization. Indeed, if there is a pure nuclear mechanism causing the fact that at high neutron energy $|M'_V| \approx 0$, $|M_V| \approx 0$, $|M'_P| \approx 0$ and $|M_P| \approx 0$, then the value $\alpha \approx -1$ could be explained in the same way.

However, nowadays no such mechanism is known. Further theoretical studies are necessary in this direction.

In conclusion the authors express their gratitude to V.G.Zinov, L.I.Lapidus, A.I.Mukhin, B.Pontecorvo, I.S.Shapiro, Yu.A.Scherbakov, for the discussion of the obtained results and I.M.Ivanchenko and A.V.Rakitsky for making calculation on the electronic computer.

Appendix

Neutron Spectrum and the Mean Energy $\bar{E}$

For the quantitative comparison of the μ^- capture theory with the experiments it is very important to know the neutron spectrum and the mean energy $\bar{E}$

when the asymmetry coefficient B is measured at a given threshold E_n of recoil protons (see the article) one can obtain a neutron spectrum and by calculating the efficiency of neutron detection $\epsilon(E, E_n)$ with the energy E with a laminated threshold detector it is possible to determine $\bar{E}$ for each E_n.

Our neutron laminated detector of low efficiency detects any particle having a range comparable with the thickness of one layer ℓ and with increasing energy E_p of the recoil proton its detection efficiency $\epsilon_p(E_p)$ will differ still greater from unity and vanish to zero. This statement as well as the principle of calculating $\epsilon_p(E_p)$ is shown in Fig.9.

Neutrons enter any layer of the neutron detector at various angles to its axis. The detector axis is perpendicular to the plane of layer separation and being continued it passes through the target centre. If one draws a plane through the direction of neutron motion perpendicularly to the surface of layer separation, then the angle of neutron entry to the element layer is ϕ (lying in this plane) between the neutron motion direction 00' and the detector axis MN. A neutron of the energy E entering at an angle ϕ to the detector layer of the thickness ℓ, produces a recoil proton at the point A. The proton emerges at an angle θ and has the energy $E_p = E\cos^2\theta$ and the range $R_p(E_p)$. For one value of the angle θ proton ranges lie at the surface of the cone having a vertex at the point A.

The efficiency $\epsilon_p(E_p)$ is determined by the value of projection II of the range $R_p(E_p)$ at the axis MN. For the given values of E, θ and ϕ (hence, also $R_p(E_p)$) there occurs some distribution $W(\Pi_i)$ of the projection Π_i at the line MN with the minimum $\Pi_{min} = LK$ and the maximum $\Pi_{max.} = LF$ values of the projection.

Proceeding from the apparatus geometry the distribution $W(\phi)$ at an angle ϕ the neutron entry to the detector (see Fig. 10) was calculated. This distribution was taken into account in plotting the projection distribution $W(\Pi_i)$ in the units R_p for a number of the angles θ :

$$W(\Pi_i) = \frac{\sum_{\phi_{min}}^{\phi_{max}} W(\phi)\, W(\Pi_i, \phi_i)}{\sum_{\phi_{min}}^{\phi_{max}} W(\phi)},$$

where $W(\Pi_i, \phi_i)$ is a range projection distribution for a fixed entry angle ϕ_i. Some of these distributions are shown in Fig. 11. For each Π_i there is its own probability ϵ_p^i of recoil proton detection

$$\epsilon_p^i(\phi, \theta, E) = \frac{\ell' - \Pi_i(\phi, \theta, E)}{\ell'}. \qquad (1)$$

In expression there is a value $\ell' = \ell + \ell_1$ where by adding ℓ_1 it is taken into account that a proton is rejected by the coincidence circuit of pulses from even and odd plates of the detector (see ref. [20]) only in the case if it passes through a translucent partition between the layers for the coincidence circuit to operate. The value ℓ_1 is equivalent to the 2.1 MeV proton range.

The total probability of detecting the recoil proton of the energy E_p or the range R_p is

$$\epsilon_p(E_p) = \frac{\sum_{\Pi_{min}}^{\Pi_{max}} \epsilon_p^i W(\Pi_i)}{\sum_{\Pi_{min}}^{\Pi_{max}} W(\Pi_i)}. \qquad (2)$$

To calculate the recoil proton spectrum $N'(E_p)$ registered in the sandwich detector for the given neutron energy E it is necessary for each E_p to obtain the product

$$\epsilon_p(E_p)\sigma_{np}(E)N''(E_p, E) = N'(E_p),$$

where $\sigma_{np}(E)$ is the cross section of elastic neutron scattering on protons and $N''(E_p,E)$ is the initial spectrum of recoil protons corrected for edge effects

To take into account edge effects the initial differential spectrum of protons $N(E_p, E)$ was separated into a number of intervals ΔE_p (or ΔR_p) and according to the detector geometry "the spread" to lower ranges was calculated for each interval. The spread was due to the fact that some protons leave the layer through a sidewall surface. Fig. 12 shows a plot of such a spread for the interval $\Delta R_p = (2.75 \div 3.0)$ g/cm^2 ($\Delta E_p = (54 \div 57)$MeV). The area of the "tail" is about 26% in this case. For all the intervals each spreaded spectrum was added to its weight and the summed spectrum was marked by $N'(E_p,E)$.

The kind of the spectrum $N(E_p)$ for various E within $(7 \div 100)$ MeV was taken from our experimental data [31]. Calculated detected spectra of recoil protons for some E_p are shown in Fig. 13.

The neutron spectrum $N_n(E)$ was determined in the following way. Taking a neutron differential spectrum N(E) which is decreased with increasing E we plotted a differential spectrum of recoil protons $N_p(E_p)$ by means of $N'(E_p,E)$ and compared it with the neutron spectrum obtained experimentally. The parameters of tested neutron spectra were varied so that the calculation curves $N_p(E_p)$ were recorded in the corridor of errors of the spectrum obtained epxerimentally.

The corridor of errors was determined both by errors in the detector energy calibration and by errors in proton counting. Two spectra giving maximum

and minimum contributions of high energy neutrons within the corridor of errors were chosen from a large number of neutron spectra. Fig. 14 shows proton spectra calculated for these two neutron spectra together with the corridor of errors. It should be noted that in this Appendix only the neutron spectrum shape was calculated but not the absolute neutron yield, and solid curves in Fig. 15 were not normalized. The points of errors in this Fig. show the neutron spectrum measured in ref. [33] and fitted from our upper curve at $E = 10$ MeV. From Fig. 15 it is seen that within errors our data on the neutron spectrum in the region of lower energies (< 15 MeV) coincide with our data [32].

Despite a great uncertainty in the spectrum at high energies even such a qualitative result is of great interest since usually a considerably faster decrease of the neutron number with increasing E takes place than it follows from data of Fig. 15.

In order to obtain so a long neutron spectrum in the independent particle model, it is necessary for its calculations to make use of the Gauss distribution [35]

$$N(p) = \exp\left[-\frac{p^2}{\alpha^2}\right], \qquad (3)$$

(p is the proton momentum) of protons in the nucleus with $\alpha = 14$ MeV [33].

To calculate the mean energy $\bar{E}$ first the efficiency $\epsilon(E, E_n)$ of neutron detection with the energy E at the threshold E_n was measured:

$$\epsilon(E, E_n) = \frac{\int_{E_n}^{E} N'(E_p, E)\, dE_p}{\int_{E_n}^{E} N(E_p, E)\, dE_p}. \qquad (4)$$

The type of $\epsilon(E, E_n)$ for some E_n is shown in fig. 16. The mean energy $\bar{E}$ is determined as

$$\bar{E} = \frac{\int_{E_n}^{100\,\mathrm{MeV}} \epsilon(E, E_n)\, E\, dE}{\int_{E_n}^{100\,\mathrm{MeV}} \epsilon(E, E_n)\, dE}. \qquad (5)$$

$\bar{E}$ was calculated for two types of curves shown in figs. 14 and 15. Thus obtained the values of $\bar{E}_{min}$ and $\bar{E}_{max}$ were used to determine $\bar{E} + \Delta\bar{E}$ given in Table 1 of the article ($\bar{E} = \frac{\bar{E}_{max} + \bar{E}_{min}}{2}$, $\Delta\bar{E} = \frac{\bar{E}_{max} - \bar{E}_{min}}{2}$).

The values of $\Delta \bar{E}$ are found mainly with a large corridor of errors in the differential proton spectrum obtained experimentally. The values of $\bar{E}$ for ΔE_n given in Table 1 are obtained in the same way.

The above calculations do not take into account neutron interactions with carbon nuclei in view of small cross sections of the reactions $C^{12}(n,n')C^{12}$, $C^{12}(np)B^{12}$, etc.[33]. The double neutron scattering in a layer detector should be considered in more detail. The double scattering on plates of different parity would cause some additional decrease of $\epsilon(E_n, E)$ whereas double scattering on plates of similar parity leads to the increase of $\epsilon(E_n, E)$ as a result of disintegration of the initial neutron energy, $\epsilon_p(E_p, E)$ being increased in each of the two scattering acts. Therefore, and also since the probability of the double scattering in plates of the same parity is in our case about 70% of the single scattering even at the lowest energy $E = 7$ MeV, this effect can be neglected.

The data on the neutron spectrum shown in Fig. 15 make it possible to determine the relative high energy neutron yield in μ^--capture in Ca. Fitting by turns our two limit curves of the neutron spectrum with the data of ref.[33] and considering that the neutron number at $E = 0$ vanishes to zero and the m maximum in the neutron spectrum is found somewhere at $E = 2$ MeV, we obtain that the fraction of neutrons of energy higher than 7 MeV and 20 MeV, respectively, is 0.44 ± 0.12 and 0.23 ± 0.09 with respect to all neutrons. The error of these values is mainly due to the inaccuracy in the determination of the neutron spectrum at high energies; the errors in the data of ref.[32] and the uncertainty in the form of the neutron spectrum at $E < 2.5$ MeV give smaller contritution to the error.

If one takes into consideration that in μ^--capture in calcium neutrons are emitted with the probability $(37 \pm 2)\%$[35], then the neutron emission rate of the energy higher than 7 MeV and 20 Mev, respectively, is 0.16 ± 0.05 and 0.09 ± 0.03 per event of μ^--capture.

References

1. И.С. Шапиро, Э.Л. Долинский, Л.Д. Блохинцев. ДАН СССР, 116, 946 (1957); Nucl.Phys., 4, 273 (1957).
2. Б.Л. Иоффе. ЖЭТФ, 33, 308 (1957).
3. K.Huang, C.Yang, T.Lee. Phys.Rev., 108, 1340 (1957).
4. L.Wolfenstein. Nuovo Cim., 7, 706 (1958).
5. H.Überall. Nuovo Cim., 6, 533 (1957).
6. Э.И. Долинский, Л.Д. Блохинцев. ЖЭТФ, 35, 1488 (1958).

7. М.К. Акимова, Л.Д. Блохинцев, Э.И. Долинский. ЖЭТФ 39, 1806 (1960).

8. W.Majewski. Acta Phys. Polon., 19, 525 (1960).

9. E.Lubkin. Ann.Phys. (New York) 11, 414 (1960).

10. С.С. Герштейн. ЖЭТФ 34, 463 (1958); А.Е.Игнатенко, Л.Б. Егоров, Д.Чултем, В.Халупа. ЖЭТФ 35, 1131 (1958).

11. C.Coffin, A.Sacks. D.Tycko. Bull.Am. Phys Soc., 3, 52 (1958).

12. A.Astbury, I.M. Blair, M.Hussain, M.A.P.Kemp, H.Muirhead, R.G.Voss. Phys. Rev. Lett., 3, 476 (1959).

13. A.Astbury, J.H.Bartley, I.M.Blair, M.A.Kemp, H.Muirhead, T.Woodhead. Preprint (1962).

14. W.Baker, C.Rubbia. Phys.Rev.Lett., 3, 479 (1959).

15. V.Telegdi. Proc. of the 1960 Annual Int. Conf. on High Energy pPhys. at Rochester, p. 713 (1960).

16. В.С. Евсеев, В.И. Комаров, В.Куш, В.С.Роганов, В.А.Черногорова, М. Шимчак. Acta Phys.Polon., 21, 313 (1962).

17. В.С. Евсеев, В.С. Роганова, В.А. Черногорова, Чжан Жунь-ва, М. Шимчак. Труды международной конференции по физике высоких энергий в Женеве, стр. 425 (1962).

18. В.С.Евсеев, В.С.Роганов, В.А. Черногорова, Чжан Жунь-ва, М. Шимчак. Phys.Lett. 6, 332 (1963).

19. В.С. Евсеев, Ф. Кильбингер, В.С. Роганов, В.А. Черногорова, М. Шимчак. Доклад на международной конференции по физике высоких энергий в г. Дубне, 1964 г.

20. В.С. Евсеев, В.И. Комаров, В. Куш, В.С. Роганов, В.А. Черногорова. М. Шимчак. Acta Phys. Polonica, 19, 675 (1960), ПТЭ, №1, 68 (1961).

21. I.Sens. Phys.Rev., 113, 679 (1957).

22. H. Morinaga, W.F.Fry. Nuovo Cim., 10, 308 (1953).

23. H.C.Evans, E.H.Bellamy. Proc.Phys.Soc., 74, 483 (1959). M.Gettner, W.Selove. Rev. Sci. Instr., 31, No. 4, 450 (1960).

24. S.Lokanthan, I.Steinberger. Nuovo Cim., (Suppl.), 2, ser. 10, 151 (1955).

25. E.W.Anderson, J.E.Rothberg. Bull.Am.Phys.Soc., 10, 80 (1955); E. E.W. Anderson. Preprint NEVIS 136, May, 1965.

26. H.Primakoff. Rev.Mod.Phys., 31, 802 (1959).

27. R.Klein, T.Neal, L.Wolfenstein. Preprint (1964).

28. Л.Д. Блохинцев, Э.И. Долинский. ЖЭТФ, 41, 1868 (1961).

29. М.Л. Иовнович, В.С. Евсеев. Phys.Lett., 6, 333 (1963).

30. S.Weinberg. Phys.Rev., 112, 1375 (1958).

31. В.С. Евсеев. Препринт ОИЯИ, Е-1457 (1963).

32. "Экспериментальная ядерная физика" (под редакцией Э. Сегре), том. 1 И.Л. 1955, стр. 436, 437.

33. D.E.Hagge, J.S.Baijal, J.A.Diar, S.N.Kaplan, R.V.Pyle. Preprint (1965).

34. Атлас нейтронных сечений (изд. второе). Атомиздат, (1959).

35. B.Macdonald, J.A. Diaz, S.N.Kaplan, R.V.Pyle. Preprint UCRL-11243, March 1965.

Received by Publishing Department on December 25, 1965.

Table 1

E_n, MeV,	ΔE_n, MeV	$\bar{E}$, MeV	$-B$	χ^2	$-B/P_\mu$
6.7±0.5		18±1	0.053±0.012	14.6	0.250±0.063
10.3±0.8		22±1.5	0.100±0.016	10.1	0.48 ±0.09
13.0±1.0		30±5	0.120±0.020	6.8	0.57 ±0.10
16.8±1.3		43±12	0.163±0.025	7.5	0.78 ±0.15
17.8±1.5		47±13	0.222±0.026	6.0	1.05 ±0.15
20.7±1.7		53±15	0.214±0.040	5.8	1.02 ±0.21
	7.9±13	21±1.5	0.076±0.020	9.0	0.36 ±0.10
	13.0±17.5	36±9	0.104±0.041	7.2	0.50 ±0.20
	17.5±20.7	50±14	0.186±0.052	6.1	0.89± 0.26

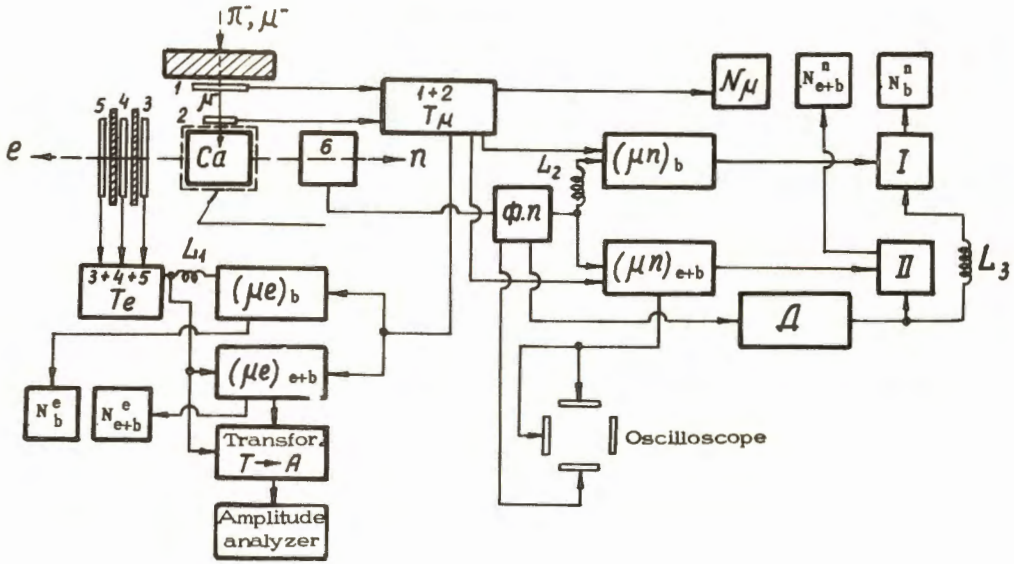

F i g. 1. The block-diagram of the experimental technique.

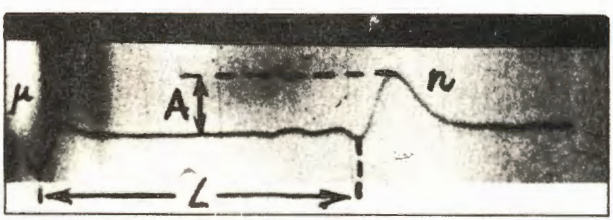

F i g. 2. A picture of the oscilloscope screen.

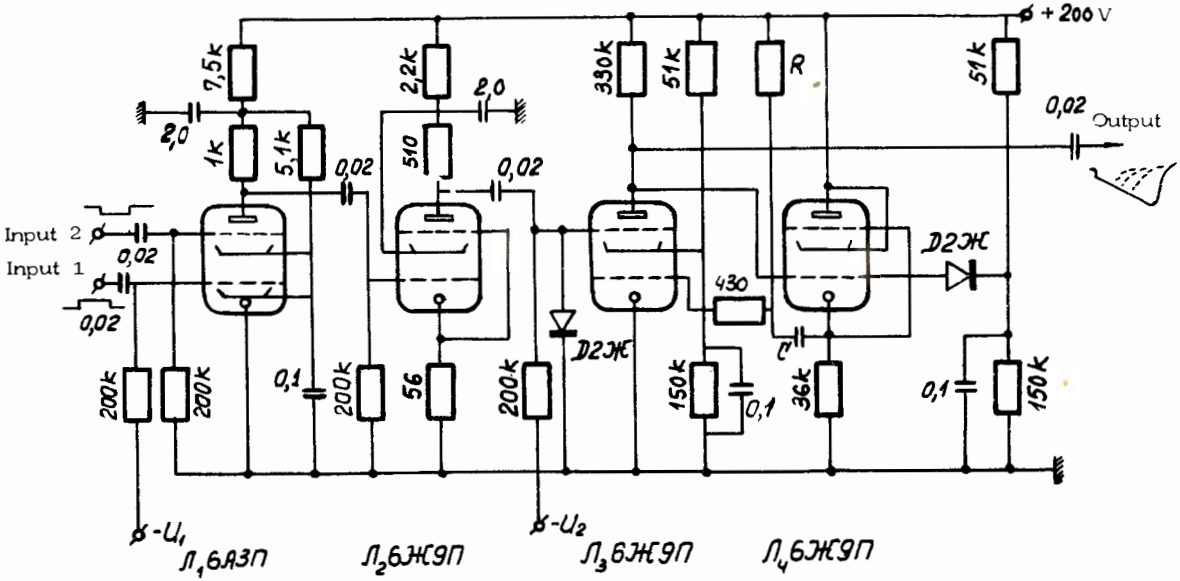

Fig. 3. A principal circuit of the time-to-amplitude convertor (T→A)

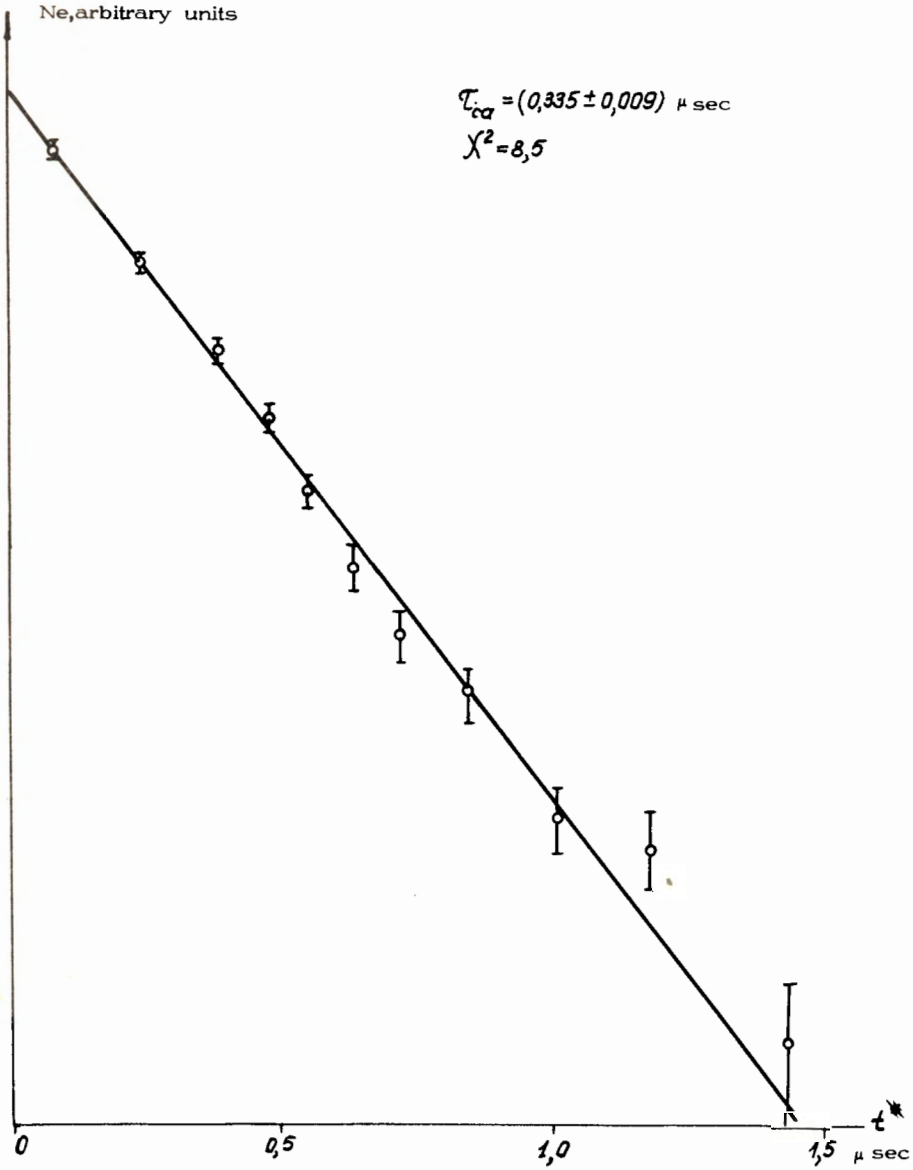

Fig. 4. The dependence of the decay electron counting rate upon the time t after the μ^- meson stopping.

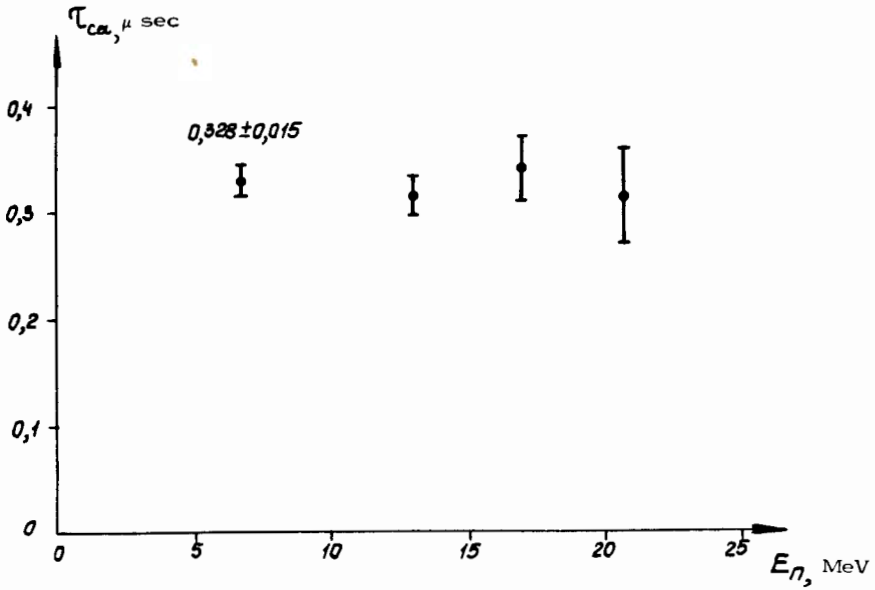

Fig. 5. The dependence of the μ^--meson life time in Ca τ_{Ca} upon the neutron detection threshold E_n

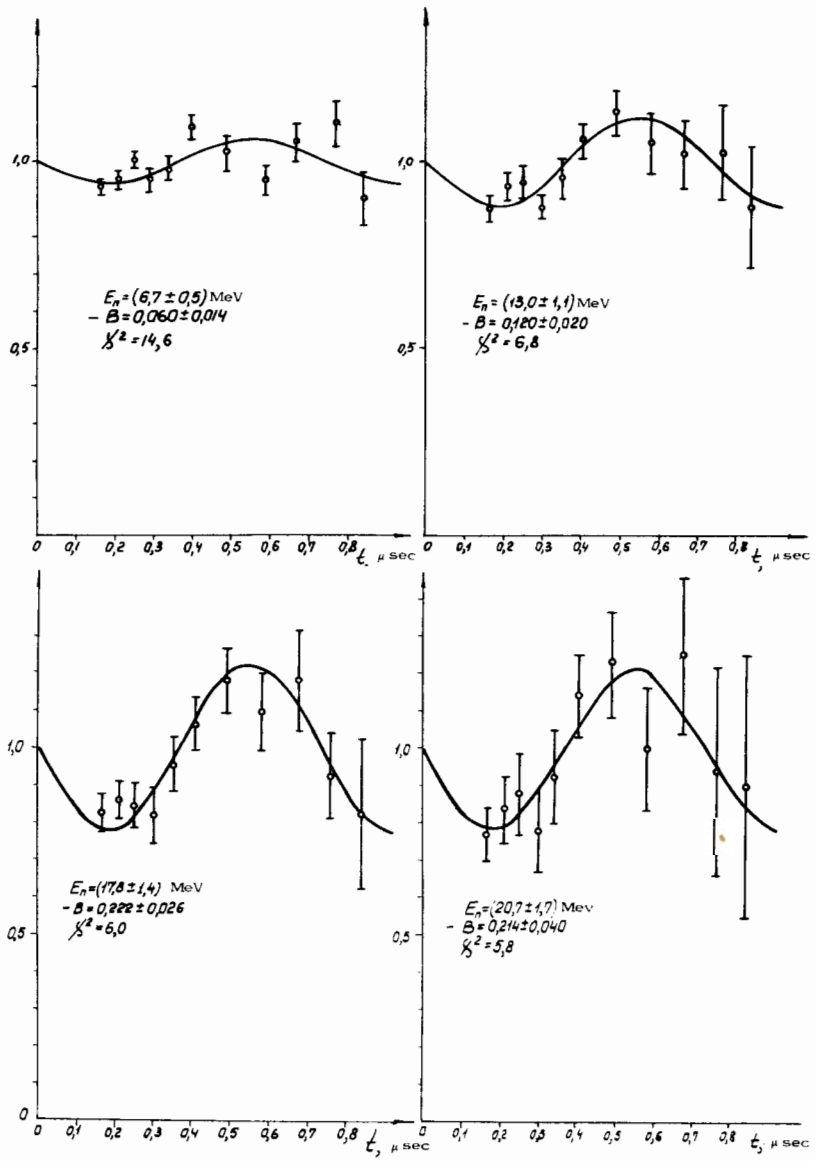

Fig. 6. Precession curves for some threshold E_n. The value $\frac{N_i - C}{N_0 \exp[t_i / \tau_0]}$ is at the ordinate axis in all the diagrams.

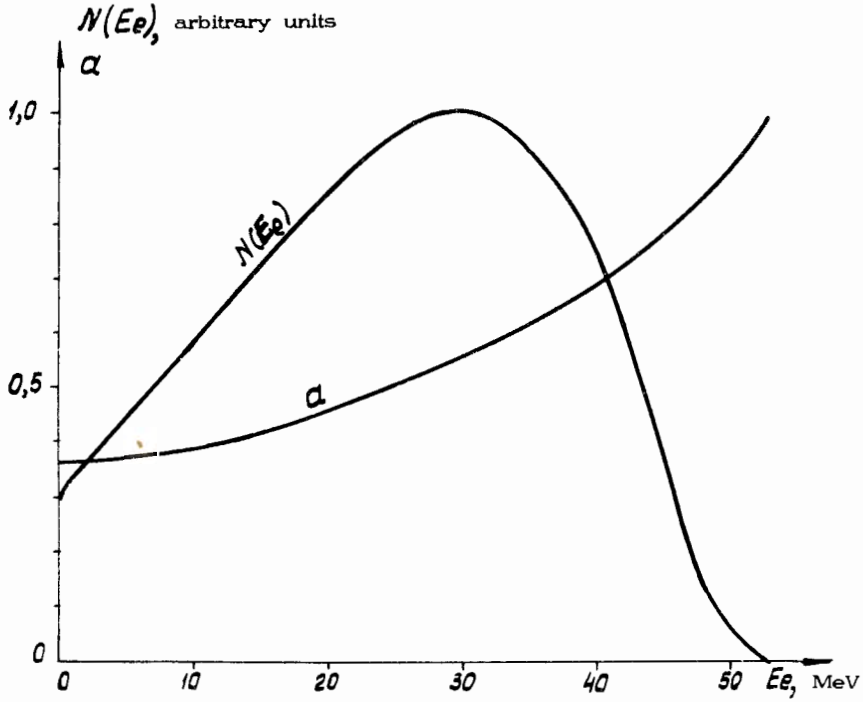

Fig. 7. Differential spectrum of decay electrons from a thick Ca target and the integral spectrum of the asymmetry coefficient in the angular distribution of decay electron at this target.

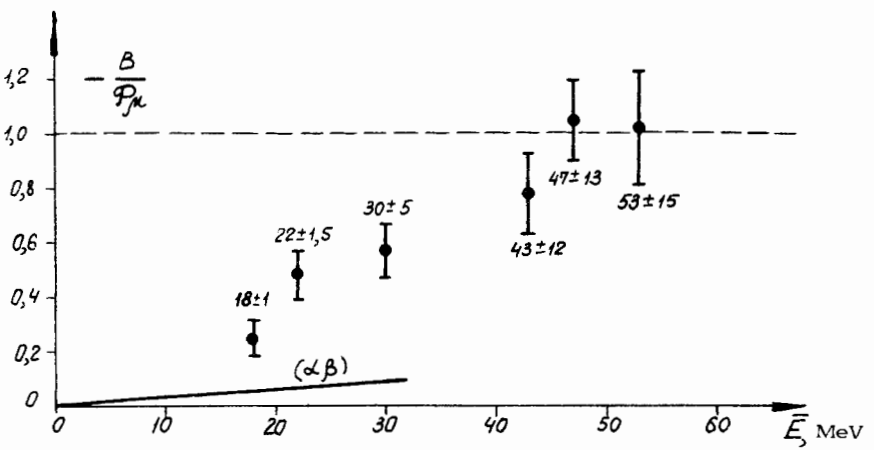

Fig. 8. Dependence of the asymmetry coefficient upon the mean energy $\bar{E}$.

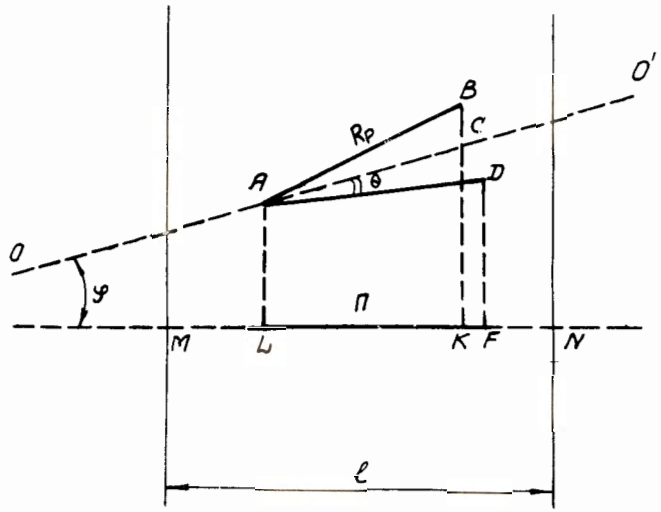

F i g. 9. Geometry of elastic (np)-scattering in the layer of the thickness ℓ.

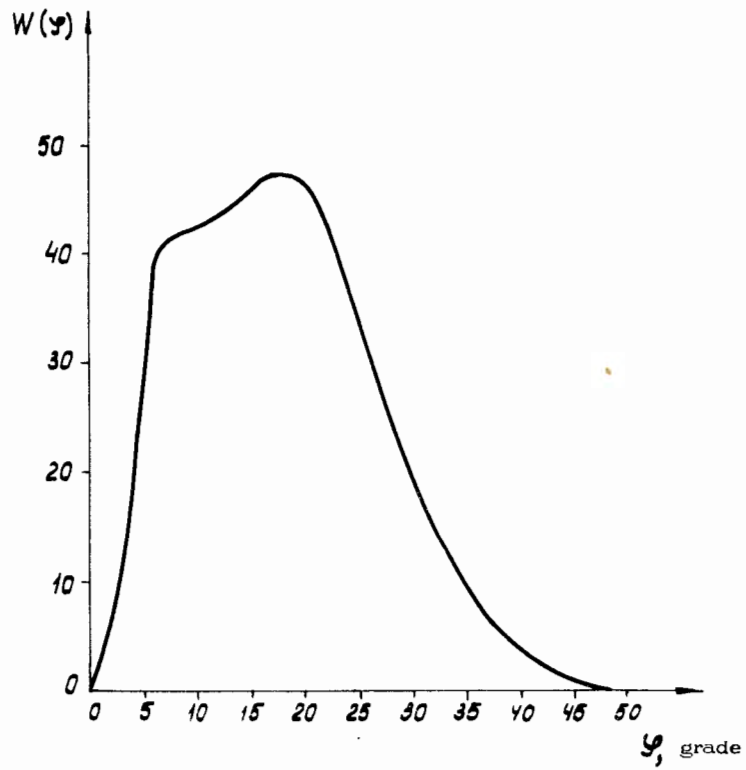

F i g. 10. The form of the $W(\phi)$ distribution according to the entrance angles.

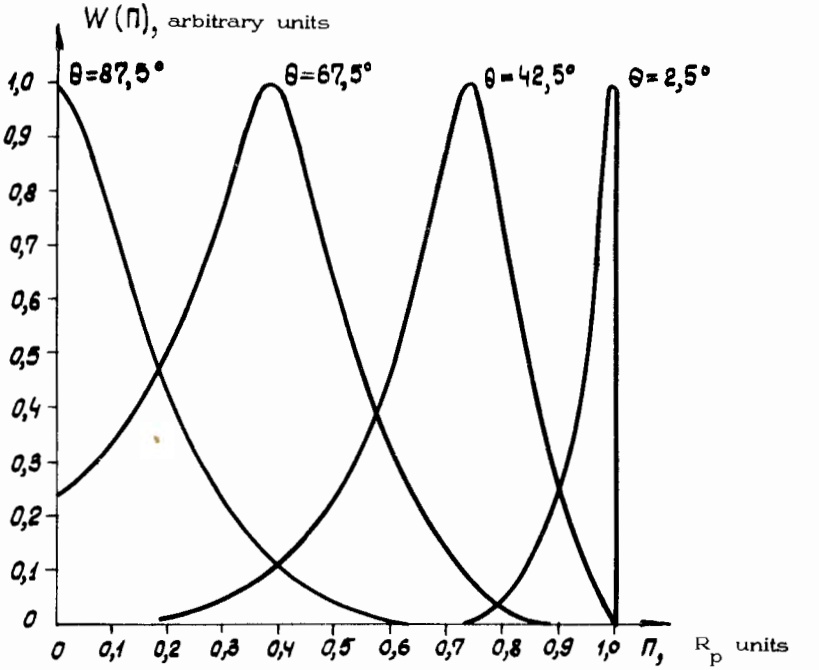

F i g. 11. The distribution W(Π) according to the projection value Π for some angles θ. All the curves are normalized to the same value W(Π) at the maximum.

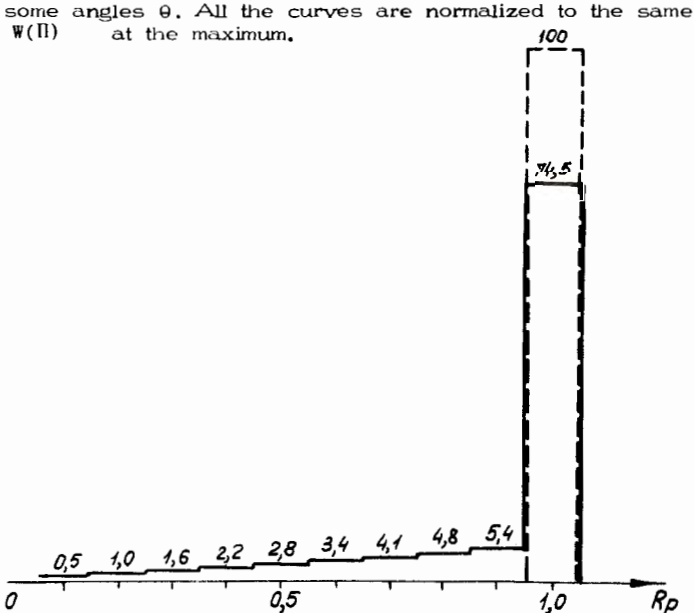

F i g. 12. The edge effect for the interval $\Delta R_p = (2.7 \div 3.0)$ g/cm^2. The figures above the hystogram show a relative column area. The dashed line is an undistorted interval.

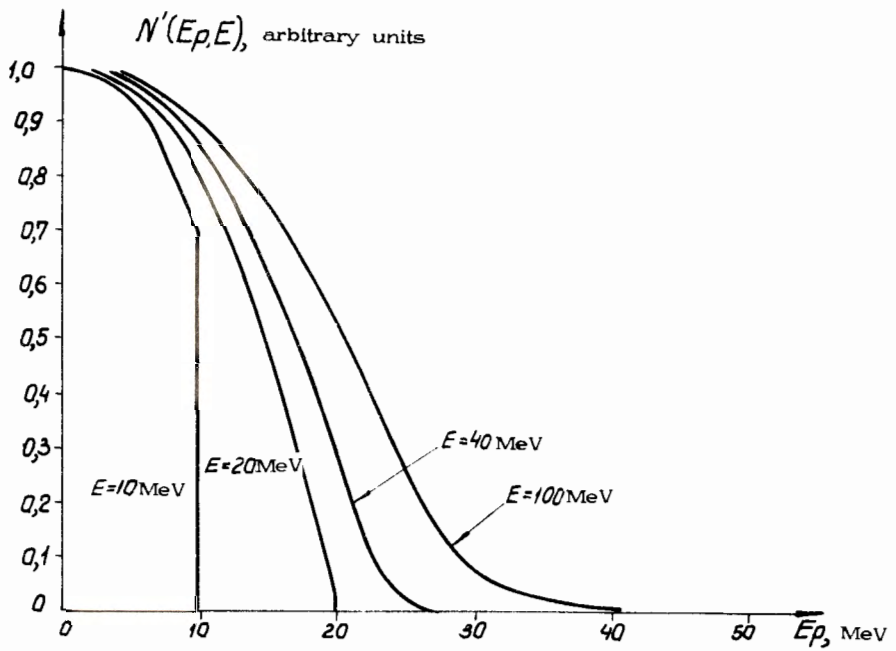

Fig. 13. Recoil proton spectra $N'(E_p, E)$ for some values of E normalized to unity with $E = 0$.

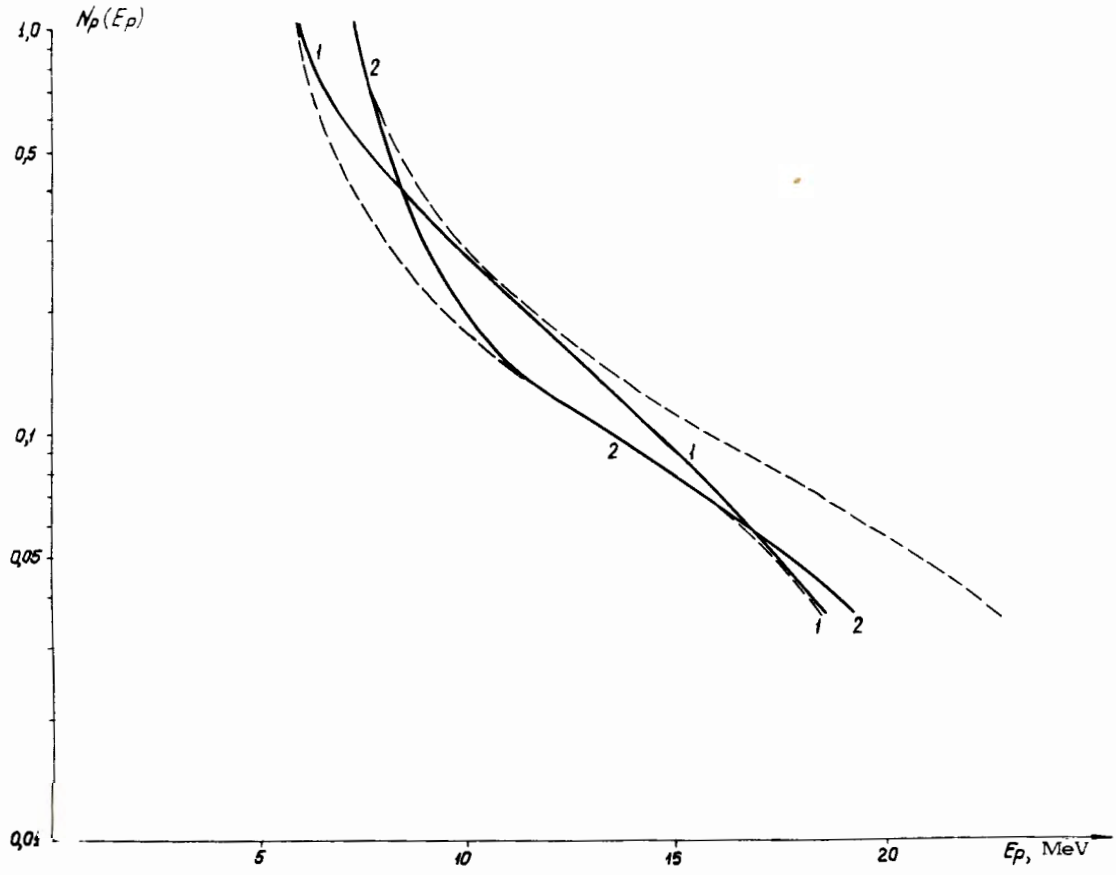

Fig. 14. The corridor of errors in measuring the differential proton spectrum with a sandwich detector (the dashed line) and two proton spectra obtained for neutron spectra with the maximum contribution of high energy neutrons (the solid curve) and for the neutron spectrum with the minimum contribution of high energy neutrons (curve 2).

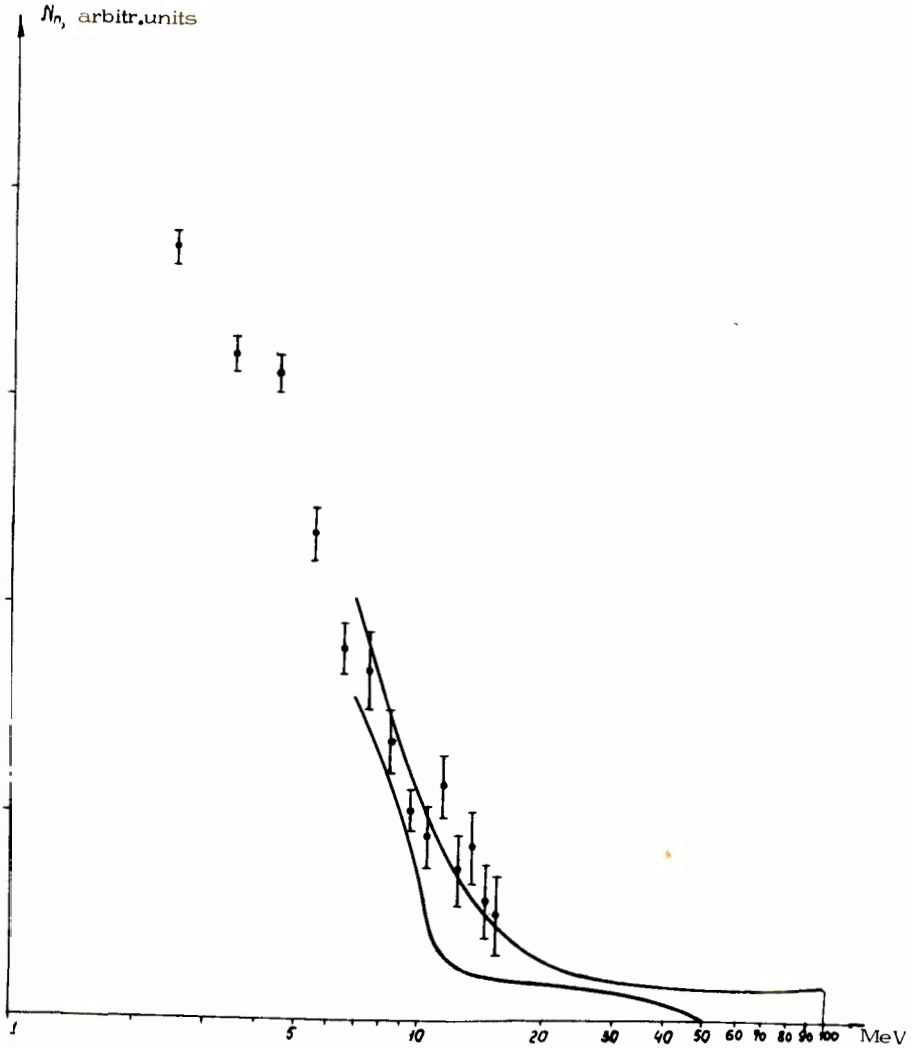

Fig. 15. Neutron spectrum from μ^--capture in ^{Ca}. The upper solid curve gives the maximum contribution of high energy neutron, the lower one gives the minimum contribution. Dots are the results of ref /33/.

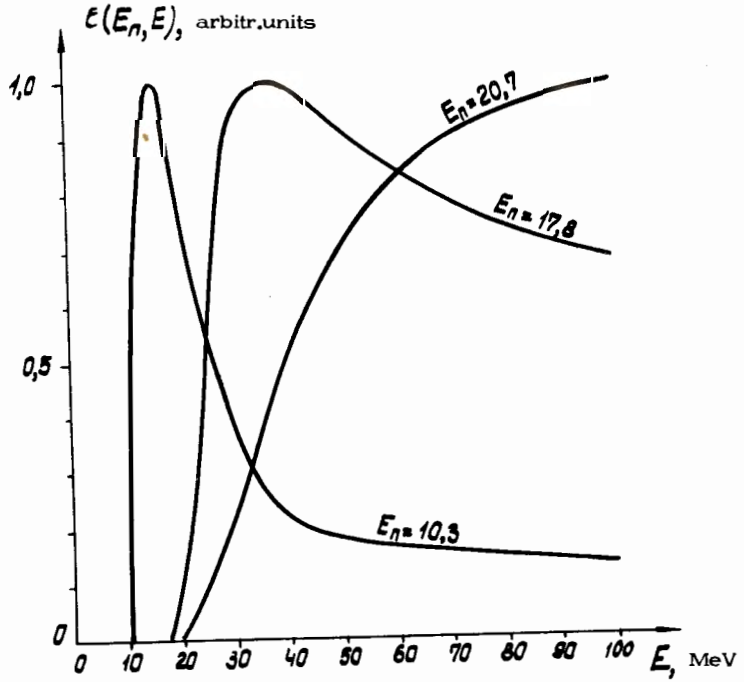

Fig. 16. Neutron detection efficiency $\epsilon(E, E_n)$ for some E_n.